Multidimensional Modelling for the Carotid Artery Blood Flow

S. A. Urquiza [a] P. J. Blanco [a] M. J. Vénere [b] R. A. Feijóo [c,*]

[a] *Laboratorio de Bioingeniería, Universidad Nacional de Mar del Plata, Av. J.B. Justo 4302, 7600 Mar del Plata, Argentina, Email: SantiagoUrquiza@fi.mdp.edu.ar*

[b] *PLADEMA–CNEA, Facultad de Exactas, Universidad Nacional del Centro de la Provincia de Buenos Aires, Pinto 399, 7000 Tandil, Argentina, Email: venerem@exa.unicen.edu.ar*

[c] *L.N.C.C, Laboratório Nacional de Computação Científica, Av. Getulio Vargas 333, Quitandinha, 25651-075, Petrópolis, RJ, Brasil, Email: feij@lncc.br*

Abstract

In this work, a multidimensional 3D–1D FEM model of the whole arterial tree is implemented. It comprises a 3D compliant model of the carotid bifurcation coupled with a 1D model for the remaining part of the arterial tree. With this approach, difficulties arising from the treatment of boundary conditions for the 3D model are naturally handled. The Navier–Stokes equations are used as the governing equations for the blood flow while an elastic compliant model is implemented for the arterial wall. Also, the A.L.E. formulation is considered within the 3D blood regions taking into account the domain deformations produced by the moving artery wall. This 3D model is complemented with a 1D model of the entire arterial tree, in order to appropriately set inflow and outflow boundary conditions for the former. The reduced 1D model solves the momentum and continuity equations in compliant tubes so as to reproduce the propagation of the pressure pulse in the arterial network. Also, a volumetric flow rate is imposed at the inlet to model the systolic work of the heart. The peripheral arteriole beds are simulated with the well known lumped Windkessel model. A standard geometry of the Carotid bifurcation is discretized with P1 bubble–P1 tetrahedral elements. The obtained results properly reproduce the general flow patterns reported in the literature. Very good agreement between the outcomes of a pure 1D model and those of the combined multidimensional model was obtained. It is worth noting that this kind of model may provide useful information for early detection and prevention of related arterial diseases.

Key words: Hemodynamic, fluid–structure interaction, FEM, coupling 3D–1D.

1 Introduction

Arterial vessel trees perform the vital task of efficiently supplying blood to all organs and tissues of the body, carrying nutrients and removing catabolic products. Hemodynamic simulation studies have been frequently used to gain a better understanding of functional, diagnostic and therapeutic aspects of the blood flow. These simulations usually employ compartmental representations or branching tube models of arterial trees as their geometrical substrate[1,25–28,30] -specially to model large extended zones- whereas localized three–dimensional models have been often implemented to study arterial flow in more detailed aspects[4,8,21,24,32].

Blood flow studies in the carotid artery bifurcation are of great clinical interest with respect to both, the genesis and the diagnostics of atherosclerotic diseases. It is well known[14] that the flow separation region of the carotid sinus has the propensity to develop atherosclerotic plaques. In this sense, the local hæmodynamic structure is intimately related to atherogenesis onset and progress[2] as low shear stress regions are associated with the development of stenotic plaques. Consequently, localized atherosclerotic lesions must be related to local flow conditions. Moreover, a deeper understanding and better descriptions of the flow structure in such a kind of vascular district ought to be of the greatest importance for the early detection of this type of arterial stenoses.

Several local 3D in vitro and computational flow models have been implemented, revealing the complex flow structure in the carotid sinus district. Bharadvaj et. al.[33,34] defined a standard geometry of the carotid bifurcation (an average over 57 actual geometries from different subjects) and conducted stationary studies of the internal carotid blood flow. They found a region of low velocities near the non-dividing wall that extend with increasing Reynolds number. Conversely, the opposite region showed large axial velocities and shear stresses. These results were confirmed by Rindt et. al.[4] using experimental and computational stationary models. Ku and Giddens[5–7] observed a similar process in 3D models during the accelerating period of the diastole and also, the existence of velocities disturbances during the decelerating phase and at the onset of the diastole. Some similar experiments have been conducted in compliant models[15].

To perform focused numerical and in vitro realistic experiments on a district such as the carotid bifurcation, special attention must be paid on the boundary conditions applied to the model. As the pressure differences between inlet and outlet boundaries are only a small percentage of the systolic–diastolic pulse

* Corresponding author.
Email address: feij@lncc.br (R. A. Feijóo).

amplitude, this imposes the problem of accurately determine the pressure, a condition that is difficult to reach in practice. In this way, small errors in the imposed pressure could lead to great departure of the velocities from the actual values. Conversely, if flow is imposed as boundary condition at the inlet and outlet of the analyzed zone, negligible variations on these values could lead to exaggerated low or high pressures. Accurate enough measures of those variables are very difficult or very costly to obtain simultaneously at the inflow and outflow regions for an entire cardiac period, even more in a noninvasive way. This in turn, leads to implement full models of the arterial tree in order to avoid artificial boundaries in the vicinity of the analyzed zone. Three–dimensional models of the whole arterial tree are, at the present times, not realizable as computational costs well exceed capabilities of modern computers and also, since it is a very compromised task to obtain and manage all the information (geometric and physiologic) necessary to construct such detailed models. Consequently, it is an interesting idea to model localized zones with great detail as 3D districts coupled with a 1D model -for the remaining part of the arterial tree- that serves as a boundary conditions provider to the former. This leads to a reduction in the number of parameters involved and also the overall complexity is substantially decreased.

Recently, the coupling and integration of models with different dimensionality have been analyzed by Quarteroni et. al.[17–22], linking together lumped models with 3D models of the arterial tree. This task is very cumbersome since this problem involves deformable domains (compliant arterial walls) as well as other nonlinearities in the governing equations such as convective terms, fluid–structure interactions and also, regions of diverse dimensionality and the coupling conditions between them. The authors have proposed elsewhere[12] an alternative approach for coupling models of non-matching dimensionality and used it to implement a model of stenoses in the common carotid artery. In this work, it is implemented a multidimensional 3D–1D model of the whole arterial tree which includes a 3D finite element model of the carotid bifurcation coupled with a 1D model for the remaining part of the arterial tree. Flow patterns for an entire cardiac period are obtained and analyzed in order to gain insight in the complexity of the unsteady flow in that region and also to evaluate the computational requirements for an accurate representation of the phenomena. Furthermore, flow rate and pressure curves at the inlet and outlet of the bifurcation are analyzed in order to show the compatibility of a pure 1D model with the coupled multidimensional model presented here.

2 The model

2.1 Governing equations

A compliant model of the whole arterial tree was developed. It comprises a 3D model of the carotid bifurcation embedded in a 1D representation for the rest of the arterial tree. The governing equations for the 1D portion of the arterial system are derived from a reduced Navier–Stokes model. This leads to the following hyperbolic set of nonlinear partial differential equations:

$$\frac{\partial Q}{\partial t} + \frac{\partial}{\partial x}\left(\alpha \frac{Q^2}{A}\right) = -\frac{A}{\rho}\frac{\partial P}{\partial x} - \frac{\pi D}{\rho}\tau_o \tag{1}$$

$$\frac{\partial A}{\partial t} + \frac{\partial Q}{\partial x} = 0 \tag{2}$$

with

$$\alpha = \frac{\int_A u^2\, dA}{Q^2} \tag{3a}$$

$$\tau_o = f_r \frac{\rho \tilde{u}|\tilde{u}|}{8} \tag{3b}$$

$$Q = \tilde{u}A \tag{3c}$$

where A is the artery cross sectional area, u the axial velocity ($\tilde{u}$ the corresponding mean value), x the axial coordinate, P the mean pressure, ρ the blood density, τ_o the viscous shear stress acting on the arterial wall with f_r a Darcy friction factor (in this work a fully developed parabolic velocity profile is considered) and α is a correction factor for the axial momentum.

Taking into account the compliance of the arterial walls, a closure equation relating the pressure to the cross sectional area is implemented:

$$P = P_{\mathrm{o}} + \frac{E h_{\mathrm{o}}}{R_{\mathrm{o}}}\left(\sqrt{\frac{A}{A_{\mathrm{o}}}} - 1\right) \tag{4}$$

where a linear relationship between P and R is considered, being R the radius of the artery, E an effective Young modulus, h the thickness of the arterial wall and the subscript 'o' denotes quantities evaluated at the reference pressure P_{o}.

The former system of equations is discretized using a Galerkin Least Squares method for the normal equations of the hyperbolic system[13].

The local 3D fluid dynamics was described using the 3D time–dependent Navier–Stokes equations for incompressible Newtonian fluids considering an

A.L.E. method[29] in order to take into account the deformability of the domain:

$$\rho\frac{\partial \mathbf{u}}{\partial t} + \rho\left(\mathbf{u}-\mathbf{v}\right)\nabla\mathbf{u} - \mu\nabla^2\mathbf{u} + \nabla P = \mathbf{f} \tag{5a}$$

$$\mathrm{div}\mathbf{u} = 0 \tag{5b}$$

$$\nabla^2\Delta\mathbf{x} = 0 \tag{5c}$$

where $\mathbf{u}$ is the fluid velocity, $\mathbf{v}$ is the moving reference frame velocity consistent with the A.L.E. formulation, P is the pressure, $\Delta\mathbf{x}$ is the displacement vector of the moving domain from its reference configuration, $\mathbf{f}$ are the volume distributed forces, ρ and μ stand for the constant fluid density and the dynamic viscosity, respectively. This set of equations must be supplied with appropriate boundary conditions and closure equations. As the domain moves with the arterial wall, a relationship representing the arterial wall displacement must be provided. Moreover, this relationship must be compatible with the 1D model in order to avoid spurious reflections at the interfaces between zones of diverse dimensionality. The simplest model that accomplishes these requirements is that of "independent rings"[15]. This was implemented via the following equations valid for points on the surface $\partial\Omega_{\mathrm{w}}$ that represents the arterial wall (see figure 1):

$$P - P_{\mathrm{o}} = \frac{Eh}{R_{\mathrm{o}}^2}\delta \tag{6a}$$

$$\Delta\mathbf{x} = \delta\,\mathbf{n} \tag{6b}$$

$$\mathbf{v} = \frac{\mathrm{d}\Delta\mathbf{x}}{\mathrm{d}t} \tag{6c}$$

where δ is the displacement of the arterial wall in the normal direction of the surface ($\mathbf{n}$ is the unit normal vector to the surface). The eq. (6a) is analogous to that of the 1D model given in eq. (4)

Another group of equations must be considered to appropriately set the coupling between the 1D and the 3D models at the interface surfaces. Continuity of mass, momentum and tractions must be imposed. For the Reynolds numbers prevailing at the carotid artery, continuity on tractions can be replaced by continuity on pressure. Consequently, continuity of blood flow is enforced at the interfaces between 1D and 3D zones jointly with weak continuity for pressures (see reference [12] for additional details). With these considerations the corresponding coupling equations result as follows:

$$Q_i = -\int_{\partial\Omega_i} \mathbf{u}.\mathbf{n}\ \mathrm{d}S \tag{7a}$$

$$\left\langle \rho\frac{\partial \mathbf{u}}{\partial t}, \mathbf{w} \right\rangle + \langle \rho\left(\mathbf{u}-\mathbf{v}\right)\nabla\mathbf{u}, \mathbf{w}\rangle - \langle P, \mathrm{div}\mathbf{w}\rangle + \langle \mu\nabla\mathbf{u}, \nabla\mathbf{w}\rangle = \langle \mathbf{f}, \mathbf{w}\rangle + \sum_i \int_{\partial\Omega_i} -P_i\mathbf{n}.\mathbf{w}\ \mathrm{d}S \qquad \forall \mathbf{w} \in \mathrm{H}^1, i = 1,2,3 \tag{7b}$$

where P_i is the mean pressure value as given by the 1D model at the 3D–1D coupling interface $\partial\Omega_i$, and Q_i is the corresponding 1D arterial blood flow output. The equation (7a) states for the continuity of mass, while equation (7b) is the variational counterpart of eq. (5a) which implies the weak continuity of pressure since Neumann boundary terms were replaced by the mean pressure as given by the 1D model.

This is a very simple and efficient alternative to coupling zones of diverse dimensionality in comparison with those proposed in [18]. With the present solution scheme, the 1D model is solved jointly with the 3D zones avoiding costly subdomain decomposition. Observe that the unknowns associated to the 1D portion of the model are not significant when compared with the total number of unknowns. Furthermore, the 3D portion of the system is responsible for the major part of the computational costs, mainly due to its greater dimensionality. Notice that momentum continuity is implied in the correct choice of the parameter α in eq. (3a), that must be evaluated nonlinearly from the results of the 3D model. Here we have used $\alpha = 1$ constant, in this way the former requirement is not completely fulfilled. However, it must be noted that relaxing this condition does not produce significant spurious reflections in the case of long wavelengths, as is in the present situation.

2.2 Numerical approach

For the numerical solution of the 3D flow problem the Finite Element Method was applied: the approximation makes use of P1–P1 bubble tetrahedral elements with linear enriched interpolation functions for the velocity vector field and linear pressure[16].

The equations are solved using the Finite Element SUPG[31] method with implicit Euler backward differences for time derivatives and Picard iteration for nonlinear convection terms. The solution of the time–dependent 3D Navier–Stokes equations is performed in two sub-steps: in the first one, the bubbles degrees of freedom are eliminated by direct substitution, and in the second one, those unknowns are updated as necessary for the evaluation of the second

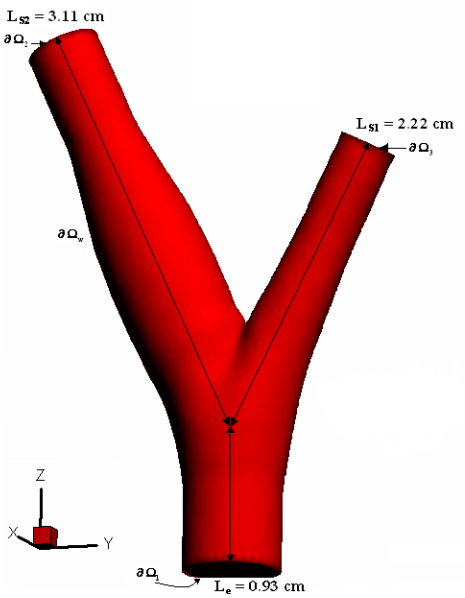

Fig. 1. 3D carotid bifurcation geometry model

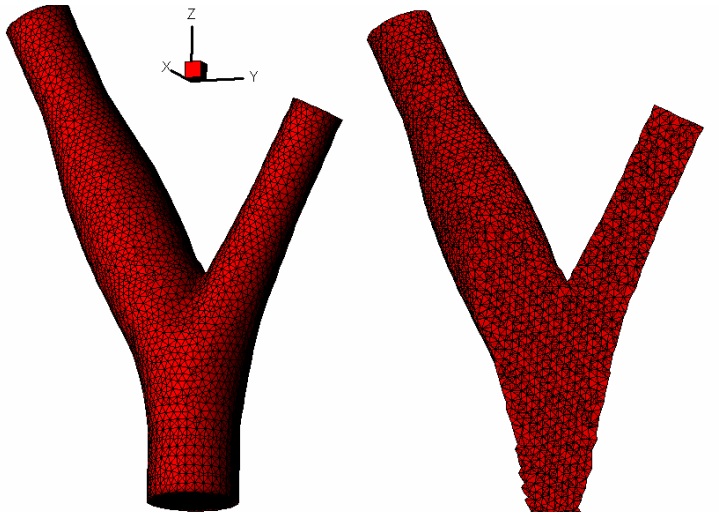

Fig. 2. 3D FEM mesh -tetrahedral elements-

member of the first set of equations at the following time step. The deformation of the domain is accounted through a Laplace equation for the displacement of the mesh -again, tetrahedral linear elements are used- where boundary displacements at the arterial wall are given by the eq. (6a).

Flow velocity patterns were calculated for a carotid artery bifurcation geometry proposed by Bharadvaj et. al.[33,34] scaled to match the Common Carotid diameter of the 1D model (0.74 mm). The resulting geometry is shown in figure 1. The corresponding 3D mesh used in the calculations is exposed in figure 2, it has 14,159 nodes and 71,732 tetrahedral elements.

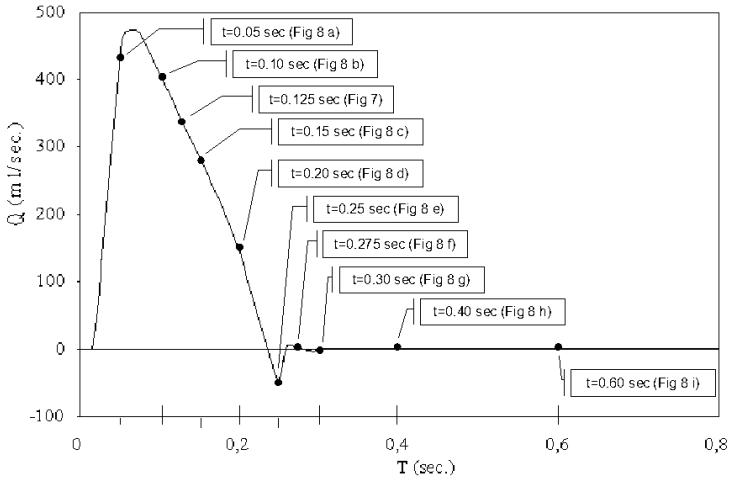

Fig. 3. Inflow boundary condition

The one–dimensional model was described in detail elsewhere [13] . It is discretized with a mesh comprising 686 nodes, 642 elements and considering three degrees of freedom per node (A, P, Q). The inlet boundary condition describing the heart blood flow is shown in figure 3. It has a period $T = 0.8$sec and was obtained from [23].

Table 1
Windkessel terminals

N°	Name	R1	R2	C
		dyn.sec.cm^{-2}.ml^{-1}		ml.cm^2.dyn^{-1}
1	Coronary	10.00E3	41.00E3	0.7900E-5
2	Intercostals	2.78E3	11.12E3	0.1638E-4
3	Gastric, Hepatic & Esplenic	2.54E3	10.17E3	0.2967E-3
4	Renal(two)	1.26E3	5.04E3	0.1235E-3
5	Superior mesenteric	1.92E3	7.68E3	0.1726E-3
6	Inferior mesenteric	16.62E3	66.46E3	0.7400E-4
7	Internal iliac	17.04E3	68.17E3	0.6750E-4
8	Deep femoral	11.60E3	46.39E3	0.5030E-5
9	Anterior tibial	56.15E3	224.61E3	0.4170E-5
10	Posterior tibial	9.54E3	38.16E3	0.3900E-5
11	Vertebral	16.65E3	66.60E3	0.9880E-4
12	Interosseous	211.74E3	846.96E3	0.3107E-6
13	Ulnar	10.56E3	42.24E3	0.3520E-5
14	Radial	10.56E3	42.24E3	0.3520E-5
15	Carotid	6.31E3	25.55E3	0.1330E-5

The model is complemented with lumped Windkessel representations for the peripheral arteriole beds. The geometry and other parameters involved are shown in figure 4 and also in tables (1,2), see reference [13] for additional details. Some minor modifications are introduced here in order to match the

Table 2
Geometric and rheologic values of the arterial segments

N°	Name	Lenght [cm]	Proximal Radius [cm]	Distal Radius [cm]	Eh [dy.cm^{-1}]
1	Ascending aorta A	1.0	1.46	1.46	741500
2	Ascending aorta B	3.0	1.45	1.45	741500
3	Aortic arch A	2.0	1.12	1.12	741500
4	Aortic arch B	3.9	1.07	1.07	576200
5	Thoracic aorta A	5.2	1.0	1.0	545640
6	Thoracic aorta B	10.4	0.675	0.675	394000
7	Abdominal aorta A	5.3	0.61	0.61	370500
8	Abdominal aorta B&C	2.0	0.6	0.6	348000
9	Abdominal aorta D	10.6	0.58	0.58	352400
10	Abdominal aorta E	1.0	0.52	0.52	252500
11,31	Common iliac	5.8	0.37	0.37	368150
12,32	External iliac	14.4	0.32	0.32	148700
13,33	Femoral	44.3	0.26	0.26	230900
14,34	Posterior tibial	33.1	0.25	0.25	667500
15	Innominate	3.4	0.62	0.62	377000
16,17	Subdavian A	3.4	0.423	0.423	288700
18,19	Subdavian B	42.2	0.403	0.403	1170000
20,21	Ulnar A	6.7	0.215	0.215	679100
22,23	Ulnar B	17.1	0.203	0.203	717664
24	Right Common carotid	20.8	0.37	0.37	264000
25	Left Common carotid	19.87	0.37	0.37	264000
26	Right External carotid	17.7	0.177	0.177	259000
27	Left External carotid	15.48	0.21	0.21	302504
28,35	Anterior tibial	34.3	0.13	0.13	513145
29,30	Radial	23.5	0.174	0.174	682580
36	Right Internal carotid	17.7	0.177	0.177	259000
37	Left Internal carotid	14.59	0.2627	0.2627	378130

diameters and lengths of the 1D model to those used in the 3D representation of the carotid bifurcation for the left external and internal carotid arteries. Finally, the selected values for ρ and μ were 1.04gr/cm^3 and 0.04Poise respectively.

The whole model was computationally implemented in a numerical framework[11] that allows to easily integrate different kinds of elements as "plug and play" without modifying the main program, i.e., the programmer only must provide the elemental matrices and organize the input in such a way that all run together. The linear equations are solved by a preconditioned (LU incomplete descomposition from SparseKit[10]) Conjugated Gradient Square method[9], although similar performance can be obtained with BCG Stabilized[10]. The cardiac period ($T = 0.8$sec) was divided into two equal intervals.

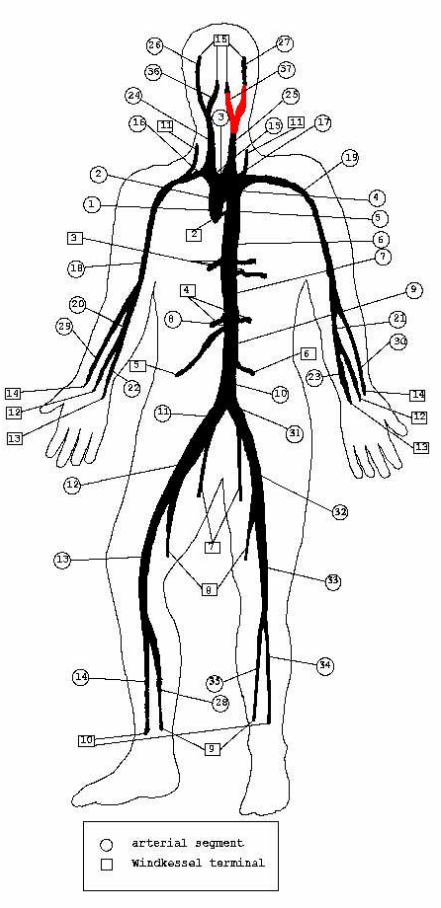

Fig. 4. Arterial tree scheme

For the systolic subperiod, a time step of $2.5E-3$sec was used, and for the diastolic one was selected a time step of $5E-3$sec . In this way, a very efficient and cost effective solver of the problem was implemented, making possible to obtain the results in a one day run on a PC platform.

3 Results

Here we present some illustrative plots at selected times. In general, the flow has a very complex and unsteady structure showing an early back flow due to the inversion of the pressure gradient at the peak of the systole (figure 6).

A considerable deformation of the artery volume can be observed in figure 5 where volume differences during diastole (red shaded) and systole (black wire frame) are displayed.

As can be seen in figure 7, a zone of low velocities near the non-divider wall of the carotid sinus is observed and contrariwise, a high velocity region occurs

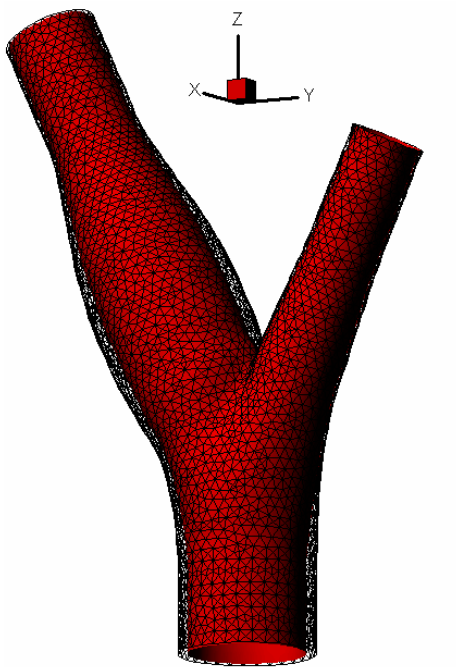

Fig. 5. Volume difference between systole and diastole

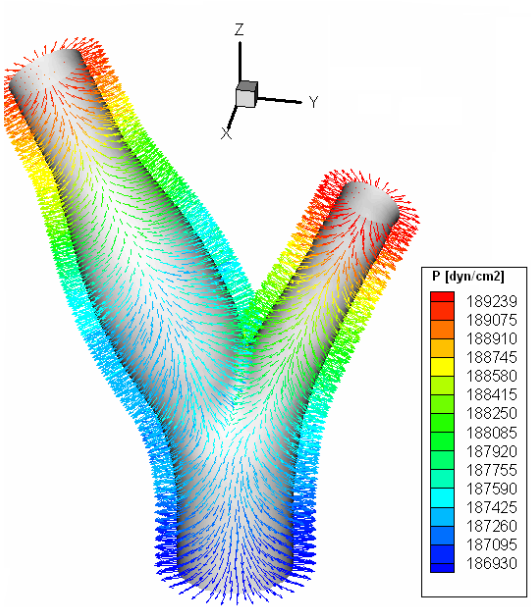

Fig. 6. Normal stress during systole at $t = 0.05$sec -inverse pressure gradient-

near the divider wall. These results agree with those obtained experimentally and numerically in references [8,15,33,34]. Detailed inspection of the computational results (see figures 8(a)-8(i)) displays the general characteristics occurring in the carotid sinus, a period with reverse axial flow starts at the peak of the systole and remains until the beginning of the diastole. This is illustrated for the V_z component of the velocity vector during the decreasing phase of the systole as shown in figure 9. Also in that figure can be observed a typical

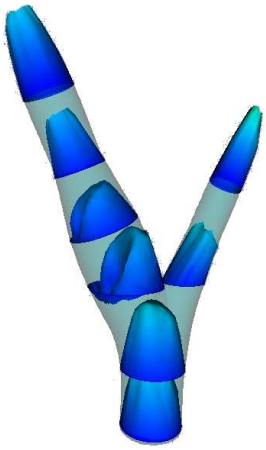

Fig. 7. Velocity during systole, $t = 0.125$sec

Womersley flow at the entrance, where the flow reversal occurs at the outer ring while at the center the velocity remains positive. In figures 10(a)-10(i) the obtained computational velocity profiles at the entrance of the common carotid are presented.

Also the outflow velocity profile for the internal and external carotid was integrated over the duration of the cardiac cycle and compared with that for the inflow condition, resulting in a conservation of mass higher than the 99.5%.

With the aim of examining the consistency of the multidimensional coupled model with regard to a pure 1D model, flow rate and pressure curves are compared. This is carried out by plotting results at the inlet and at the outlets of the 3D districts. Figure 11(c) shows those quantities for the inlet, whereas figure 11(a) and 11(b) show the same for both outlets. Also from these plots, the non–dimensional L^2 norm for the differences between values corresponding to the coupled model and the pure 1D model was evaluated, resulting in errors lower than 2% for all cases.

4 Conclusions

A computational model that face the problem of simulating compliant 3D arterial districts coupled with a 1D model of the rest of the arterial tree was presented. The resulting scheme has shown excellent capabilities to deal with considerable domain deformations while preserving the computational efficiency. Calculations of the flow field for the carotid artery are in general agreement with those reported previously in the literature, for both experimental and numerical cases[6–8,15,24]. The consistency of the coupled model was also shown by computing flow rate and pressure curves at the coupling

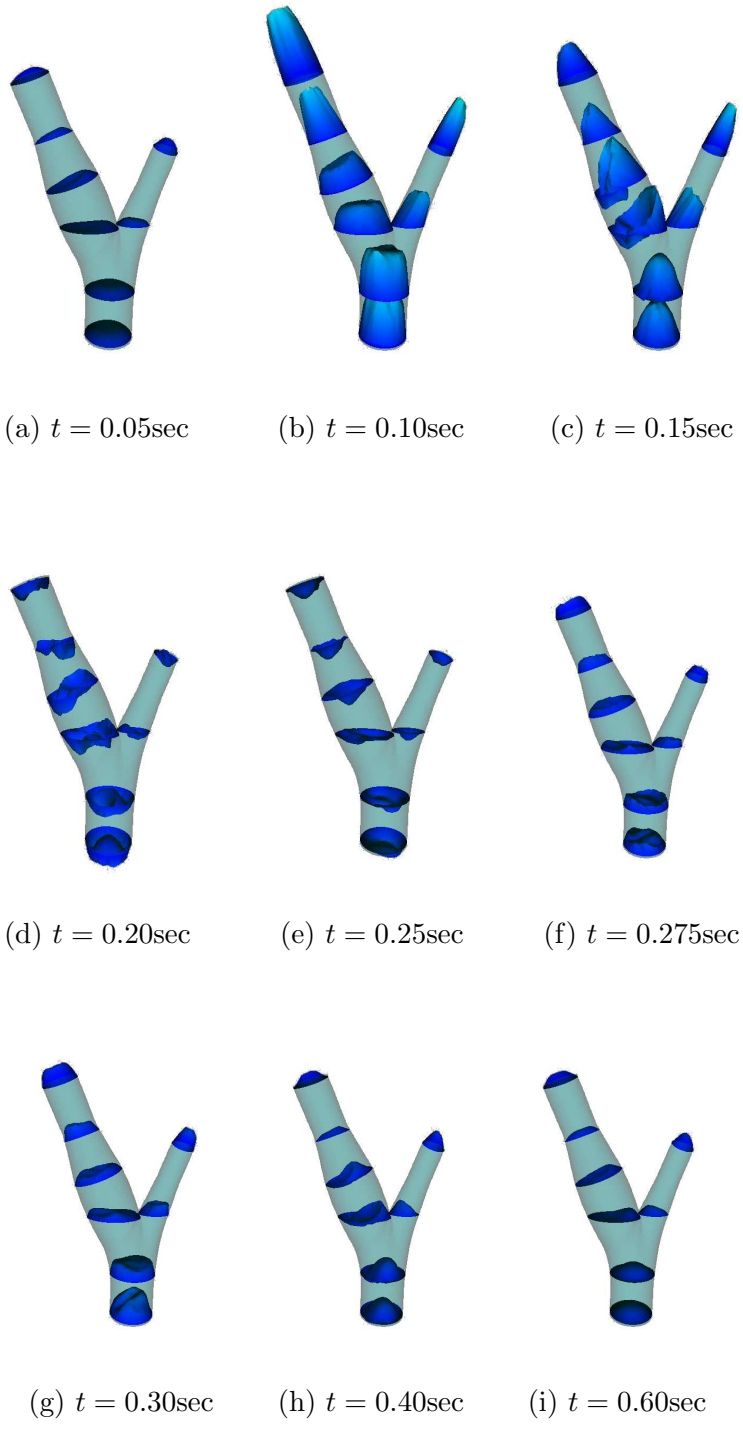

(a) $t = 0.05$sec (b) $t = 0.10$sec (c) $t = 0.15$sec

(d) $t = 0.20$sec (e) $t = 0.25$sec (f) $t = 0.275$sec

(g) $t = 0.30$sec (h) $t = 0.40$sec (i) $t = 0.60$sec

Fig. 8. Velocity profiles

boundaries and comparing these results with those of a pure 1D model. Finally, this class of model can be of valuable aid as it takes into account more realistic boundary conditions when studying 3D zones of the arterial tree, a fact that can contribute to gain insight on the flow patterns that influence the

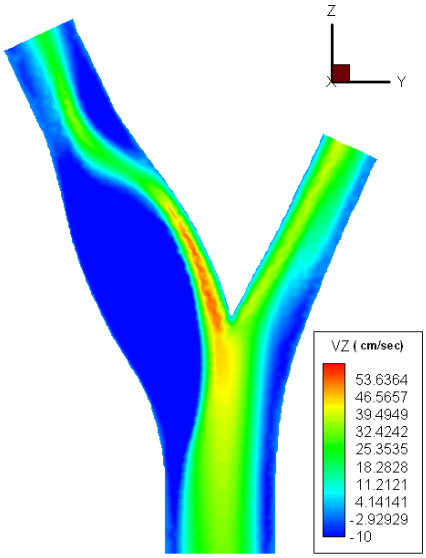

Fig. 9. Back flow during late systole, $t = .18$sec

start and development of atherosclerotic disease.

Acknowledgements

This research was partly supported by FINEP/CNPq-PRONEX Project under Contract 664007/1997-0, by MCT/PCI-LNCC Project, CNPq-Grant 304850/2003-9 and by CONICET (Argentina). The support from these agencies is greatly appreciated.

References

[1] P. Bruinsma, T. Arts, J. Dankelman, J.A.E. Spaan, Model of the coronary circulation based on pressure dependence of coronary resistance and compliance, *Basic Res. Cardiol.* **83** (1988) 510–524.

[2] C.G. Caro, J.M. Fitz-Gerald, R.C. Schroter, Atheroma and arterial wall shear dependent mass transfer mechanism for atherogenesis, *Proc. Royal Society of London, Biology,* **B177** (1971) 109–159.

[3] F.J.H Gijsen et. al., Analysis of the axial flow field in stenosed carotid artery bifurcation models: LDA experiments, *Journal of Biomechanics* **29** (1996) 1483–1489.

[4] C.C.M. Rindt, A.A. Steenhoven, J.D. Van Janssen, R.S. Reneman, A. Segal, A numerical analysis of steady flow in a three-dimensional model of the carotid artery bifurcation, *Journal of Biomechanics* **23** (1990) 461–473.

[5] D.N. Ku, D.P. Giddens, Hemodynamics of the normal carotid bifurcation, *Ultrasound in Medicine and Biology* **11** (1985) 13–26.

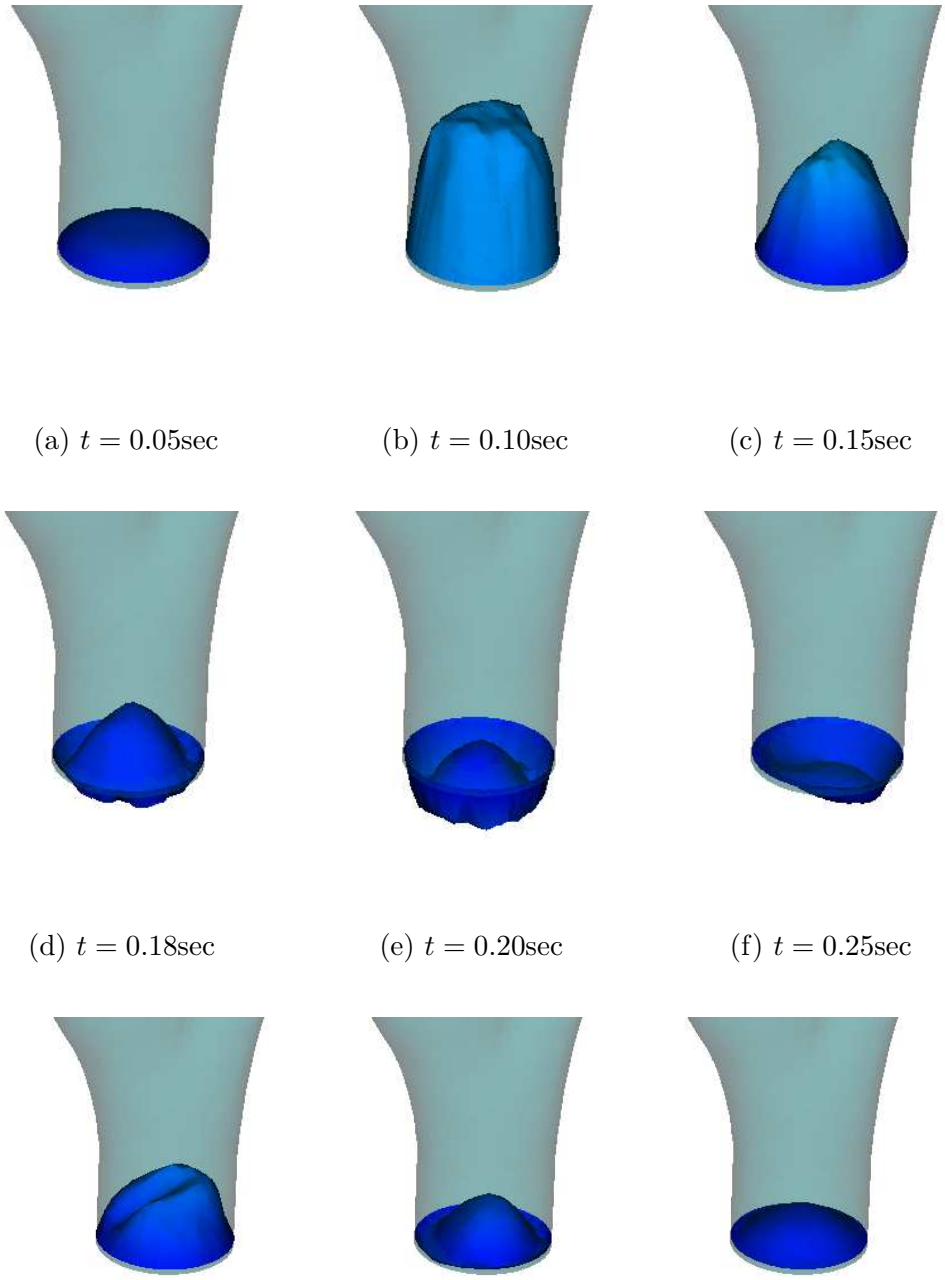

(a) $t = 0.05$sec (b) $t = 0.10$sec (c) $t = 0.15$sec

(d) $t = 0.18$sec (e) $t = 0.20$sec (f) $t = 0.25$sec

(g) $t = 0.30$sec (h) $t = 0.40$sec (i) $t = 0.60$sec

Fig. 10. Velocity profiles at the entrance of the common carotid

[6] D.N. Ku, D.P. Giddens, Laser Doppler anemometer measurements of pulsatile flow in a model carotid bifurcation, *Journal of Biomechanics* **20** (1987) 407–421.

[7] D.N. Ku, D.P. Giddens, C.K. Zarins, S. Glagov, Pulsatile flow and atherosclerosis in the human carotid bifurcation, *Arteriosclerosis* **5** (1985) 293–

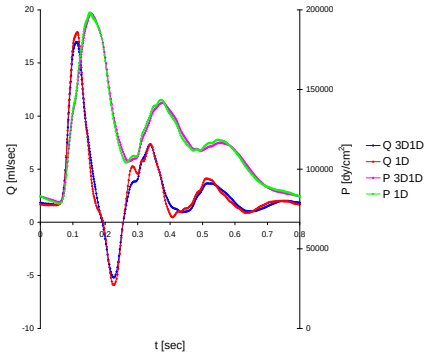

(a) Major outlet

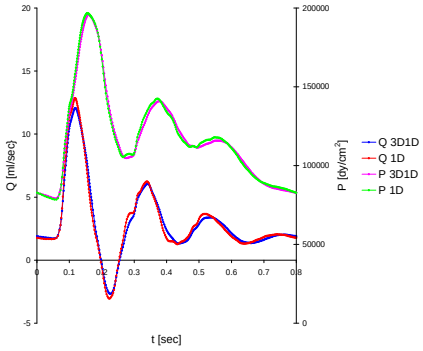

(b) Minor outlet

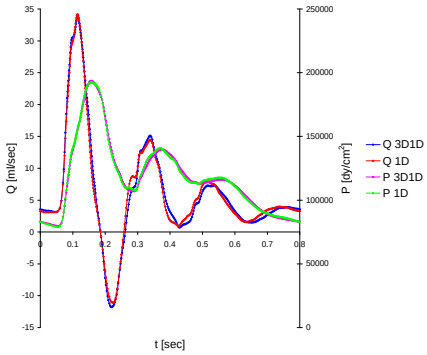

(c) Inlet

Fig. 11. Flow rate and pressure curves at the interfaces

302.

[8] R.H. Botnar, G. Rappitsch, M.B. Scheidegger, D. Liepsch, K. Perktold, P. Boesiger, Hemodynamics in the carotid artery bifurcation: a comparison between numerical simulations and in vitro MRI measurements, *Journal of Biomechanics* **33** (2000) 137–144.

[9] P. Sonneveld et. al., Multigrid and Conjugate Gradient Methods as convergence acceleration techniques, *Multigrid Methods for Integral and Differential Equations* (Clarendon Press, Oxford, 1985).

[10] Y. Saad, SPARSEKIT: a basic tool kit for sparse matrix computation version 2, http//:www-users.cs.umn.edu/˜saad/software/SPARSEKIT/sparsekit.html, University of Illinois (1985).

[11] S.A. Urquiza, M.J. Vénere, An application framework architecture for FEM and other related solvers, in: S. Idelsohn, V. Sonzogni, A. Cardona, eds., *Mecánica Computacional Vol. XXI* (CERIDE, Santa Fe, 2002) 3099–3109.

[12] S.A. Urquiza, A.L. Reutemann, M.J. Vénere, R.A. Feijóo, Acoplamiento de

modelos unidimensionales y multidimensionales para la resolución de problemas hemodinámicos, in: *proc. ENIEF 2001, XII Congress on Numerical Methods and their applications* (AMCA, Córdoba, 2002).

[13] S.A. Urquiza, M.J. Vénere, F.M. Clara, R.A. Feijóo, Finite Element (One-dimensional) Hmodynamic model of the Human Arterial System, in: E. Onate, G.Bugeda and B. Suarez, eds., *proc. ECCOMAS 2000, European Community on Computational Methods in Applied Sciences and Engineering* (Artes Gráficas Torres S.A., Barcelona, 2000)

[14] D.P. Giddens, C.K. Zarins, S. Glagov, The role of fluid mechanics in the localization and detection of atherosclerosis, *J. Biomech. Engng.* **115** (1993) 588–594.

[15] A.S. Anayiotos, S.A. Jones, D.P. Giddens, S. Glagov, C.K. Zarins, Shear stress at a compliant model of the human carotid bifurcation, *J. Biomech. Engng.* **117** (1994) 98–106.

[16] O. Pironneau, Finite element methods for fluids, (Wiley, New York, 1989).

[17] A. Quarteroni, Modelling the cardiovascular system: a mathematical challenge, in: B. Engquist, W. Schmid, eds., *Mathematics unlimited – 2001 and beyond* (Springer-Verlag, 2001) 961–972.

[18] L. Formaggia, J.F. Gerbeau, F. Nobile, A. Quarteroni, On the coupling of 3D and 1D Navier–Stokes equations for flow problems in compliant vessels, *Comp. Meth. App. Mech. Engng.* **191** (2001) 561–582.

[19] L. Formaggia, J.F. Gerbeau, F. Nobile, A. Quarteroni, Numerical treatment of defective boundary conditions for the Navier–Stokes equations, *SIAM J. Numer. Anal.* **40** (2002) 376–401.

[20] R. Pietrabissa, A. Quarteroni, G. Dubini, A. Veneziani, F. Migliavacca, S. Ragni, From the global cardiovascular hemodynamics down to the local blood motion: preliminary applications of a multiscale approach, in: E. Oate, G.Bugeda and B. Suarez, eds., *proc. ECCOMAS 2000, European Community on Computational Methods in Applied Sciences and Engineering* (Artes Grficas Torres S.A., Barcelona, 2000)

[21] A. Quarteroni, M. Tuveri, A. Veneziani, Computational vascular fluid dynamics: problems, models and methods, *Computing and Visualisation in Science* **2** (2000) 163–197.

[22] L. Formaggia, F. Nobile, A. Quarteroni,A. Veneziani, Multiscale modelling of the circulatory system: a preliminary analysis, *Computing and Visualisation in Science* **2** (1999) 75–83.

[23] J.C. Stettler, P. Niederer, M. Anliker, Theoretical analysis of arterial hemodynamics including the influence of bifurcations part I, *Annals of Biomedical Engineering* **9** (1981) 145–164.

[24] K. Perktold, G. Rappitsch, Computer simulation of local blood flow and vessel mechanics in a compliant carotid artery bifurcation model, *Journal of Biomechanics* **28** (1995) 845–856.

[25] M.F. Snyder, V.C. Rideout, R.J. Hillestad, Computer modelling of the human systemic arterial tree, *J. Biomech. Engng.* **1** (1968) 341–353.

[26] A.P. Avolio, Multi-branched model of the human arterial system, *Med. Biol. Engng. Comp.* **18** (1980) 709–718.

[27] N. Stergiopulos, D.F. Young, T.R. Rogge, Computer simulation of arterial flow with applications to arterial and aortic stenoses, *Journal of Biomechanics* **25** (1992) 1477–1488.

[28] B.W. Schaaf, P.H. Abrecht, Digital computer simulation of human systemic arterial pulse wave transmission: a nonlinear model, *J. Biomech. Engng.* **15** (1982) 349–362.

[29] T.J.R. Hughes, W.K. Liu, Zimmermann, Lagrangian–Eulerian finite element formulation for incompressible viscous flows, *Comp. Meth. App. Mech. Engng.* **29** (1981) 329–349.

[30] T.J.R. Hughes, A study of the one–dimensional theory of arterial pulse propagation, *Ph. D. Thesis, Report Number 74-13, Structures and Materials Research, Department of Civil Engineering, Division of Structural Engineering and Structural Mechanics, University of California, Berkeley* (1974).

[31] T.J.R. Hughes, A. Brooks, A theoretical framework for Petrov–Galerkin methods with discontinuos functions: Application to the stream–upwind procedure, in: R.H. Gallagher, D.M. Norrie, J.T. Oden and O.C. Zienkiewicz, eds., *Finite Element in Fuids* **IV** (Wiley, London, 1982) 46–65.

[32] C.A. Taylor, T.J.R. Hughes, C.K. Zarins, Finite element blood flow modeling in arteries, *Comp. Meth. App. Mech. Engng.* **158** (1998) 155–196.

[33] B.K. Bharadvaj, R.F. Mabon, D.P. Giddens, Steady flow in a model of the human carotid bifurcation–I. Flow visualisation, *Journal of Biomechanics* **15** (1982) 349–362.

[34] B.K. Bharadvaj, R.F. Mabon, D.P. Giddens, Steady flow in a model of the human carotid bifurcation–II. Laser–Doppler anemometer measurements, *Journal of Biomechanics* **15** (1982) 363–378.